Solar Phys
DOI 10.1007/s11207-013-0322-8

Transit Time of Coronal Mass Ejections under Different Ambient Solar Wind Conditions

A. Shanmugaraju · Bojan Vršnak

Received: 25 May 2012 / Accepted: 7 May 2013

Abstract The speed [$v(R)$] of coronal mass ejections (CMEs) at various distances from the Sun is modeled (as proposed by Vršnak and Gopalswamy in *J. Geophys. Res.* **107**, 2002, doi:10.1029/2001/JA000120) by using the equation of motion $a_{\mathrm{drag}} = \gamma(v - w)$ and its quadratic form $a_{\mathrm{drag}} = \gamma(v - w)|v - w|$, where v and w are the speeds of the CME and solar wind, respectively. We assume that the parameter γ can be expressed as $\gamma = \alpha R^{\beta}$, where R is the heliocentric distance, and α and β are constants. We extend the analysis of Vršnak and Gopalswamy to obtain a more detailed insight into the dependence of the CME Sun–Earth transit time on the CME speed and the ambient solar-wind speed, for different combinations of α and β. In such a parameter-space analysis, the results obtained confirm that the CME transit time depends strongly on the state of the ambient solar wind. Specifically, we found that: i) for a particular set of values of α and β, a difference in the solar-wind speed causes larger transit-time differences at low CME speeds [v_0], than at high v_0; ii) the difference between transit times of slow and fast CMEs is larger at low solar-wind speed [w_0] than at high w_0; iii) transit times of fast CMEs are only slightly influenced by the solar-wind speed. The last item is especially important for space-weather forecasting, since it reduces the number of key parameters that determine the arrival time of fast CMEs, which tend to be more geo-effective than the slow ones. Finally, we compared the drag-based model results with the observational data for two CME samples, consisting of non-interacting and interacting CMEs (Manoharan *et al.* in *J. Geophys. Res.* **109**, 2004). The comparison reveals that the model results are in better agreement with the observations for non-interacting events than for the interacting events. It was also found that for slow CMEs ($v_0 < 500\ \mathrm{km\,s^{-1}}$), there is a deviation between the observations and the model if slow-wind speeds ($\approx 300 - 400\ \mathrm{km\,s^{-1}}$) are taken for the model input. On the other hand, the model values and the observed data agree for both the slow and the fast CMEs if higher solar-wind speeds are assumed. It is also found that the quadratic form of the drag equation reproduces the observed transit times of fast CMEs better than the linear drag model.

A. Shanmugaraju (✉)
Department of Physics, Arul Anandar College, Karumathur 625 514, Madurai (Dist.), India
e-mail: shanmugaraju_a@yahoo.com

B. Vršnak
Hvar Observatory, Faculty of Geodesy, Kaciceva 26, 10000 Zagreb, Croatia

Published online: 30 May 2013

Keywords Sun · Coronal mass ejections · Radio bursts

1. Introduction

Coronal mass ejections (CMEs) are large-scale magnetized plasma structures most often ejected from the active regions on the Sun. The measured speeds in the plane of sky range from tens of $\mathrm{km\,s^{-1}}$ up to 3000 $\mathrm{km\,s^{-1}}$ with an average value of ≈ 450 $\mathrm{km\,s^{-1}}$ (Gopalswamy *et al.*, 2000, 2001, 2005; Yashiro *et al.*, 2004). The apparent angular width of CMEs ranges from a few degrees to more than 120 degrees, with an average value of ≈ 47 degrees (Gopalswamy, 2004).

Coronal mass ejections and their interplanetary counterparts (interplanetary CMEs or ICMEs) are the main source of major geomagnetic storms (*e.g.* Gosling *et al.*, 1990; Bothmer and Schwenn, 1995; Tsurutani and Gonzalez, 1998; Zhang *et al.*, 2003; Koskinen and Huttunen, 2006). Consequently, one of the central points of space-weather forecasting is the prediction of ICME arrival at Earth, utilizing coronagraphic observations of CMEs.

After take-off, during their propagation in interplanetary space, ICMEs accelerate/decelerate depending on their speed relative to the solar wind: slow CMEs are accelerated by the solar wind, whereas fast CMEs are decelerated (*e.g.* Gopalswamy *et al.*, 2001; Vršnak, Magdalenic, and Zlobec, 2004; Vršnak, Vrbanec, and Calogovic, 2008 and references therein). Such behavior indicates that "aerodynamic drag" plays an essential role in the propagation of ejections (*e.g.* Vršnak, 2001; Cargill, 2004; Manoharan, 2006; Borgazzi *et al.*, 2009).

In the simplest form, kinematical models used for the arrival-time predictions employ an effective constant acceleration whose value depends on the ICMEs take-off speed (most often taken to be the mean speed of a CME in the coronagraph field of view). The transit time is then calculated by assuming that such an acceleration acts up to a certain heliocentric distance, beyond which the ICME travels at constant speed (*e.g.* Manoharan *et al.*, 2004; Michalek *et al.*, 2004).

The goal of this article is to improve the accuracy of the ICME arrival-time predictions by applying kinematical modeling of the ICME propagation, where the acceleration is expressed more realistically than in the previously mentioned method. In other words, we analyze the propagation of ICMEs by solving the model equations numerically, to examine the evolution of the ICME speed. This enables evaluation of the ICME Sun–Earth transit time for various characteristics of the ambient solar wind, which is more reliable than the simple constant-velocity or constant-acceleration approach.

2. Method

Generally, the net force acting on the ICME can be written (Vršnak, 2006) as

$$F = m(a_\mathrm{L} - a_\mathrm{drag} - g), \tag{1}$$

where a_L is the acceleration due to the Lorentz force or some other driving force, a_drag is the acceleration due to solar-wind drag, and g is the acceleration due to the solar gravity.

Typically, beyond ten solar radii ($R > 10$, where $R = r/r_\mathrm{s}$ is the heliocentric distance expressed in solar radii) the acceleration due to the Lorentz force and gravity become negligible. Thus, the equation of motion reduces to

$$F = ma_\mathrm{drag}. \tag{2}$$

Vršnak and Gopalswamy (2002) proposed that the acceleration caused by the drag can be expressed in an approximate form as

$$a_1^{\mathrm{drag}} = \gamma_1 (v - w), \tag{3}$$

where v is the ICME speed, w is the distance-dependent solar-wind speed, and γ_1 is the drag parameter. In this form, the drag is proportional to the relative speed. As found from observational data, the quadratic expression in velocity

$$a_2^{\mathrm{drag}} = \gamma_2 (v - w)|v - w| \tag{4}$$

might be more appropriate, so we will consider also this quadratic-form option. Finally, we will assume that $\gamma_{1,2}$ decreases with the heliocentric distance as

$$\gamma_{1,2} = \alpha_{1,2} R^{-\beta}, \tag{5}$$

where α and β are constants (for details, see Vršnak and Gopalswamy, 2002).

Thus, considering that the driving force and the gravity are much weaker than the drag force, the interaction with the ambient solar wind can be modeled by using a simple expression for the equation of motion (Vršnak and Gopalswamy, 2002), which in linear form reads

$$\mathrm{d}v/\mathrm{d}t = -\alpha_1 R^{-\beta}(v - w). \tag{6}$$

Taking into account $v = r_\mathrm{s}\,\mathrm{d}R/\mathrm{d}t$, where r_s is the solar radius, and $\mathrm{d}v/\mathrm{d}t = (\mathrm{d}v/\mathrm{d}R)(\mathrm{d}R/\mathrm{d}t) = (\mathrm{d}v/\mathrm{d}R)v$, one finds

$$\mathrm{d}v/\mathrm{d}R = -r_\mathrm{s}\alpha_1 R^{-\beta}(1 - w/v). \tag{7}$$

Repeating the same procedure for the quadratic form, the equation of motion becomes

$$\mathrm{d}v/\mathrm{d}R = -r_\mathrm{s}\alpha_2 R^{-\beta}(1 - w/v)|v - w|. \tag{8}$$

We solved Equations (7) and (8) numerically by taking for the solar-wind speed the empirical expression proposed by Sheeley *et al.* (1997):

$$w(R) = w_0 \left(1 - \mathrm{e}^{-(R-2.8)/8.1}\right)^{1/2}, \tag{9}$$

where w_0 is the asymptotic value of the solar-wind speed. In this way we obtained the ICME speed as a function of heliocentric distance [$v(R)$], which also provides $v(t)$ and, consequently, $R(t)$.

3. Results and Discussion

3.1. ICME Speed as a Function of Distance

First, we calculated the ICME speed as a function of heliocentric distance by considering the values $\alpha_1 = 2 \times 10^{-3}\ \mathrm{s}^{-1}$, $\beta = 1.5$, and $w_0 = 400\ \mathrm{km\,s^{-1}}$. The ICME take-off speed is taken to be $1000\ \mathrm{km\,s^{-1}}$, $600\ \mathrm{km\,s^{-1}}$, $400\ \mathrm{km\,s^{-1}}$, and $200\ \mathrm{km\,s^{-1}}$ and the outcome is plotted in Figure 1. It is clearly seen in the figure that fast ICMEs ($v > w$) decelerate, whereas slow ICMEs ($v < w$) accelerate.

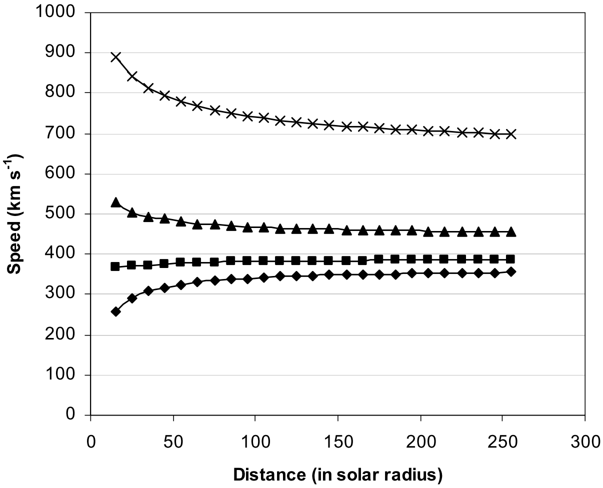

Figure 1 ICME speed *versus* heliocentric distance for different take-off speeds (cross – 1000 km s^{-1}, triangle – 600 km s^{-1}, square – 400 km s^{-1}, diamond – 200 km s^{-1}) calculated applying $\alpha_1 = 2 \times 10^{-3}\ s^{-1}$, $\beta = 1.5$, and $w_0 = 400$ km s^{-1}.

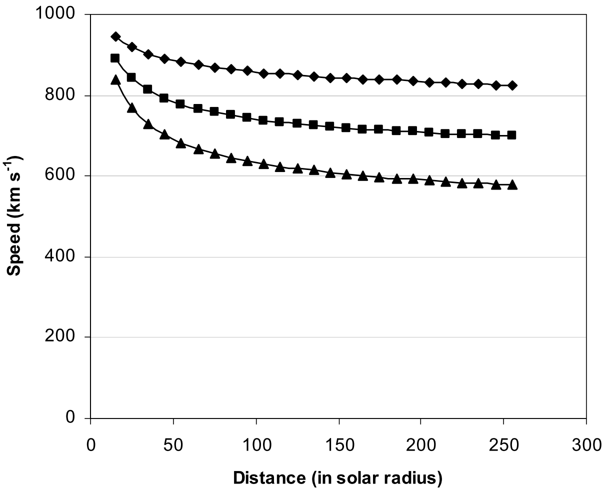

Figure 2 ICME speed [km s^{-1}] *versus* heliocentric distance for different values of α_1 (diamond – $1 \times 10^{-3}\ s^{-1}$, square – $2 \times 10^{-3}\ s^{-1}$, triangle – $3 \times 10^{-3}\ s^{-1}$), calculated applying the take-off speed of 1000 km s^{-1}, $\beta = 1.5$, and $w_0 = 400$ km s^{-1}.

Next, the evolution of ICME speed is determined for three different values of α_1 ($1 \times 10^{-3}, 2 \times 10^{-3}, 3 \times 10^{-3}\ s^{-1}$), by keeping the ICME take-off speed as 1000 km s^{-1}, $\beta = 1.5$ and $w_0 = 400$ km s^{-1}. This is important because the ambient conditions may vary from one event to another. The results are plotted in Figure 2, and it is seen that at large distances, the ICME speed decreases from roughly 800 km s^{-1} to 600 km s^{-1} when α_1 increases from 1×10^{-3} to $3 \times 10^{-3}\ s^{-1}$, respectively.

The same calculations are repeated for different values of β (1, 1.5, 2), applying the take-off speed 1000 km s^{-1}, $\alpha_1 = 2 \times 10^{-3}\ s^{-1}$, $w_0 = 400$ km s^{-1}. The outcome is presented in Figure 3. At large distances, the ICME speed increases from approximately 400 km s^{-1} to 900 km s^{-1} when β increases from 1 to 2.

The above results reveal that the evolution of speed of ICMEs in interplanetary space strongly depends on the ambient solar-wind medium (Vršnak and Gopalswamy, 2002; Vršnak and Zic, 2007). According to a recent study by Temmer *et al.* (2011) of three events by comparing the measured CME kinematics with the solar-wind models, the CME speed

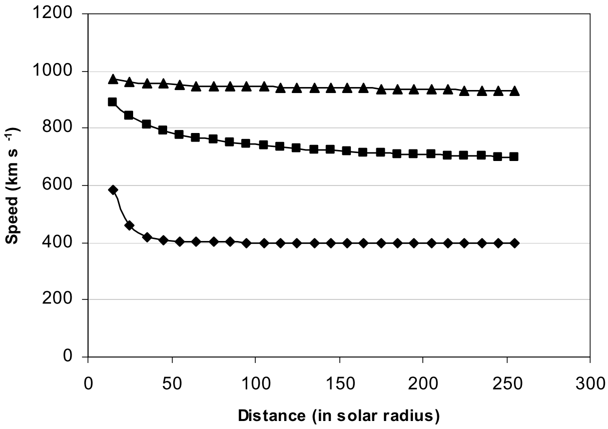

Figure 3 ICME speed *versus* heliocentric distance for different values of β (diamond – $\beta = 1$, square – $\beta = 1.5$, triangle $-\beta = 2$), calculated applying the take-off speed of 1000 $\mathrm{km\,s^{-1}}$, $\alpha_1 = 2 \times 10^{-3}\ \mathrm{s^{-1}}$, and $w_0 = 400\ \mathrm{km\,s^{-1}}$.

becomes adjusted to the solar-wind speed at different heliospheric distances: from below $30 r_{\mathrm{s}}$ to beyond 1 AU, depending on the CME and ambient solar-wind characteristics.

3.2. Transit Time as a Function of Take-off Speed

The ICME Sun–Earth transit time [$T_{1\mathrm{AU}}$] is obtained as follows. The initial heliocentric distance from which we release the ICME with a given take-off speed [v_0] is provisionally taken as $R = 10$. The Sun–Earth transit time was then found as $T_{1\mathrm{AU}} = T^1 + t^1$, where T^1 is the travel time obtained by integrating Equation (7) or (8), whereas t^1 is the time the CME needs to travel from $R = 1$ to $R = 10$ by assuming a constant-speed propagation.

Equations (7) and (8) were integrated numerically to determine the model transit times [$T_{1\mathrm{AU}}$] of ICMEs as a function of the initial velocity [v_0]. The initial velocity range $v_0 = 200 - 1500\ \mathrm{km\,s^{-1}}$ was considered. The solar-wind speed $w(R)$ described by Equation (9) was applied, taking $w_0 = 300, 400, 500$, and $600\ \mathrm{km\,s^{-1}}$. A set of values for α ($1 \times 10^{-3}, 2 \times 10^{-3}, 3 \times 10^{-3}\ \mathrm{s^{-1}}$) and β (1, 1.5, 2) was used.

The results of calculations based on Equation (7) are presented in Table 1, for a range of initial speeds $v_0 = 200 - 1400\ \mathrm{km\,s^{-1}}$ and asymptotic wind speeds ranging from 300 to 600 $\mathrm{km\,s^{-1}}$, with $\beta = 1.5$ and $\alpha_1 = 1 \times 10^{-3}\ \mathrm{s^{-1}}$. At $w_0 = 300\ \mathrm{km\,s^{-1}}$, the transit time decreases from 6.58 days for an initial speed of 200 $\mathrm{km\,s^{-1}}$, to 1.38 days for an initial speed of 1400 $\mathrm{km\,s^{-1}}$. At $w_0 = 600\ \mathrm{km\,s^{-1}}$, the transit time decreases from 4.29 days for an initial speed of 200 $\mathrm{km\,s^{-1}}$, to 1.32 days for an initial speed of 1400 $\mathrm{km\,s^{-1}}$. Thus, at these values of α_1 and β, the difference is large at low v_0, whereas there is practically no difference at high v_0. Note also that the difference between transit times of slow and fast ICMEs is larger at low w_0 than at high w_0.

This is also illustrated in Figure 4: for a particular initial speed of a CME, say 400 $\mathrm{km\,s^{-1}}$, the ICME takes 4.77, 4.25, 3.87, and 3.57 days to reach the Earth for wind speeds of 300, 400, 500, and 600 $\mathrm{km\,s^{-1}}$, respectively. On the other hand, at high v_0, there is practically no difference.

The same calculations were repeated for a different value of α ($\alpha_1 = 2 \times 10^{-3}\ \mathrm{s^{-1}}$) and the results are given in Table 2 and graphs are presented in Figure 5. The results are similar to those described earlier. However, the merging of all curves is not seen in this graph as in Figure 4.

The ICME transit times were also calculated for the quadratic velocity dependence by employing Equation (8). The outcome for $\alpha_2 = 5 \times 10^{-6}\ \mathrm{km^{-1}}$, and $\beta = 1.5$ is presented in

Table 1 Transit times calculated for $\beta = 1.5$ and $\alpha_1 = 1 \times 10^{-3}\ \mathrm{s}^{-1}$.

v_0 [km s^{-1}]	$w_0 = 300$ [km s^{-1}] T_{1AU} [days]	$w_0 = 400$ [km s^{-1}] T_{1AU} [days]	$w_0 = 500$ [km s^{-1}] T_{1AU} [days]	$w_0 = 600$ [km s^{-1}] T_{1AU} [days]
200	6.58	5.50	4.80	4.29
400	4.77	4.25	3.87	3.57
600	3.39	3.17	2.99	2.83
800	2.53	2.43	2.34	2.26
1000	1.99	1.94	1.89	1.85
1200	1.63	1.60	1.57	1.55
1400	1.38	1.36	1.34	1.32

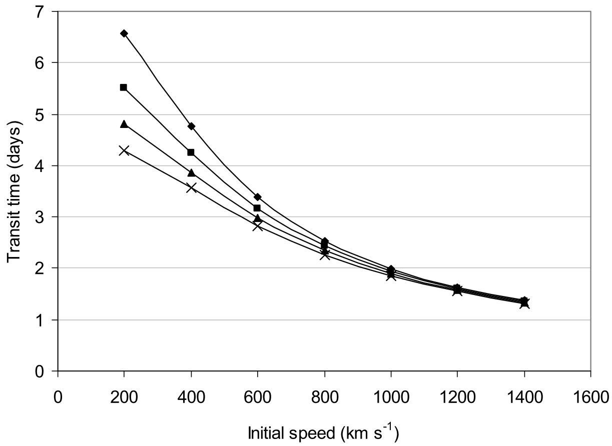

Figure 4 Sun–Earth transit time *versus* the ICME take-off speed calculated employing Equation (7) with $\alpha_1 = 1 \times 10^{-3}\ \mathrm{s}^{-1}$, and $\beta = 1.5$, for different values of solar-wind speed (diamond – 300 km s^{-1}, square – 400 km s^{-1}, triangle – 500 km s^{-1}, cross – 600 km s^{-1}).

Table 2 Transit times calculated for $\beta = 1.5$ and $\alpha_1 = 2 \times 10^{-3}\ \mathrm{s}^{-1}$.

v_0 [km s^{-1}]	$w_0 = 300$ [km s^{-1}] T_{1AU} [days]	$w_0 = 400$ [km s^{-1}] T_{1AU} [days]	$w_0 = 500$ [km s^{-1}] T_{1AU} [days]	$w_0 = 600$ [km s^{-1}] T_{1AU} [days]
200	6.07	4.84	4.08	3.56
400	5.15	4.26	3.69	3.29
600	4.00	3.48	3.11	2.84
800	3.04	2.77	2.56	2.39
1000	2.34	2.23	2.10	2.00
1200	1.91	1.83	1.76	1.69
1400	1.59	1.54	1.49	1.45

Figure 6, where one can see that the results are slightly different from the results obtained by the linear approximation especially for $v_0 > 500\ \mathrm{km\,s^{-1}}$.

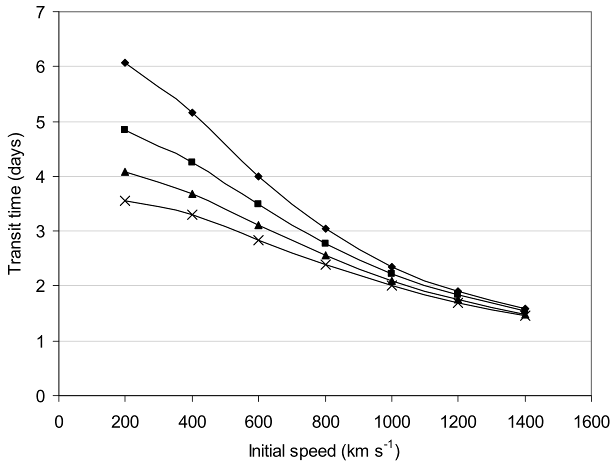

Figure 5 Sun–Earth transit time *versus* the ICME take-off speed calculated employing Equation (7) with $\alpha_1 = 2 \times 10^{-3}\ \mathrm{s}^{-1}$, and $\beta = 1.5$, for different values of solar-wind speed (diamond – $300\ \mathrm{km\,s}^{-1}$, square – $400\ \mathrm{km\,s}^{-1}$, triangle – $500\ \mathrm{km\,s}^{-1}$.

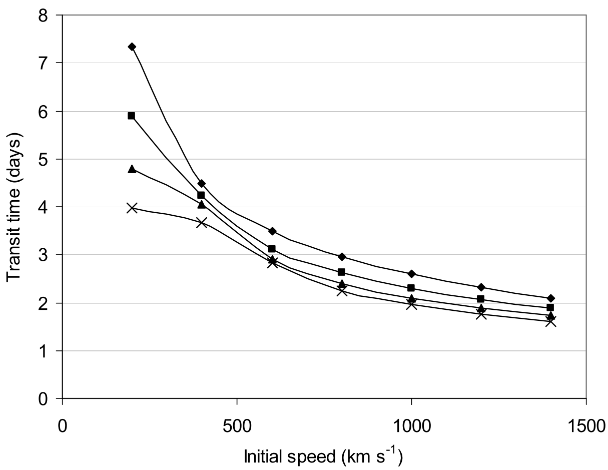

Figure 6 Sun–Earth transit time *versus* the ICME take-off speed calculated employing Equation (8) with $\alpha_2 = 5 \times 10^{-6}\ \mathrm{km}^{-1}$, and $\beta = 1.5$, for different values of solar-wind speed (diamond – $300\ \mathrm{km\,s}^{-1}$, square – $400\ \mathrm{km\,s}^{-1}$, triangle – $500\ \mathrm{km\,s}^{-1}$, cross – $600\ \mathrm{km\,s}^{-1}$).

Transit times are calculated again applying $\alpha_2 = 5 \times 10^{-6}\ \mathrm{km}^{-1}$, and $\beta = 2$, and the results are plotted in Figure 7. Here, the difference between transit times for different solar-wind speeds reduces very rapidly as the CME's initial speed increases: the transit time is almost independent of the wind speed when the initial speed is beyond $400\ \mathrm{km\,s}^{-1}$.

3.3. Transit Time as a Function of Wind Speed

The calculations performed above also provide direct information on the dependence of the ICME transit time on the solar-wind speed. The results are presented in Figure 8. As can be seen in the graph, the ICME transit time clearly reduces when the solar-wind speed increases. For example, with an initial speed of $200\ \mathrm{km\,s}^{-1}$, a CME takes nearly six days to reach the Earth in a solar-wind speed of $300\ \mathrm{km\,s}^{-1}$. But the same CME reaches the Earth in 3.5 days in a solar-wind speed of $600\ \mathrm{km\,s}^{-1}$. The transit time of a high-speed CME ($1400\ \mathrm{km\,s}^{-1}$) is only slightly influenced by the solar-wind speed, *i.e.* about $T_{1\mathrm{AU}} = 1.6$ days when the wind speed is $300\ \mathrm{km\,s}^{-1}$, whereas, it reduces to $T_{1\mathrm{AU}} = 1.5$ days when the wind speed is $600\ \mathrm{km\,s}^{-1}$. It is a similar result to Vršnak and Gopalswamy (2002) that the effect

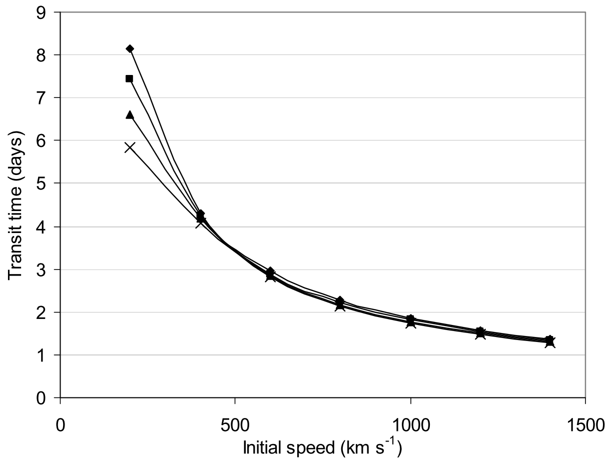

Figure 7 Sun–Earth transit time *versus* the ICME take-off speed calculated employing Equation (8) with $\alpha_2 = 5 \times 10^{-6}\ \mathrm{km}^{-1}$, and $\beta = 2$, for different values of solar-wind speed (diamond – $300\ \mathrm{km\,s}^{-1}$, square – $400\ \mathrm{km\,s}^{-1}$, triangle – $500\ \mathrm{km\,s}^{-1}$, cross – $600\ \mathrm{km\,s}^{-1}$).

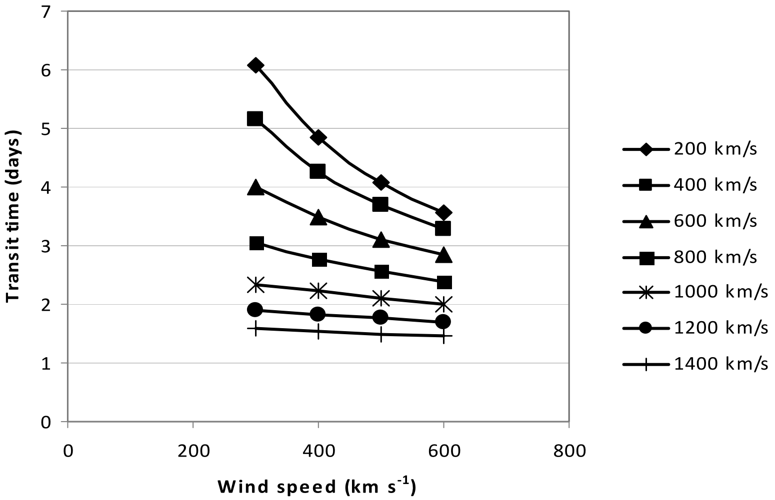

Figure 8 Sun–Earth transit time *versus* the wind speed calculated employing Equation (7) with $\alpha_1 = 2 \times 10^{-3}\ \mathrm{s}^{-1}$, and $\beta = 1.5$, for different values of ICME take-off speed.

of solar-wind drag is greater in the case of CMEs with low v_0 than for CMEs with high v_0. As suggested by Vršnak *et al.* (2010), the shortest transit times and accordingly the highest 1 AU velocities are related to narrow and massive ICMEs propagating in high-speed solar-wind streams. On the other hand, wide ICMEs of low masses adjust to the solar-wind speed close to the Sun, so the transit time is determined primarily by the solar-wind speed.

3.4. Comparison with Observations

We consider a set of 90 events employed by Manoharan *et al.* (2004) and the ICME initial speeds and transit times estimated therein. Out of 90 events, 25 events were classified as interacting events. Hence, we have separated the events into non-interacting and interacting ICMEs, and compared the values from Manoharan *et al.* (2004) with the results based on

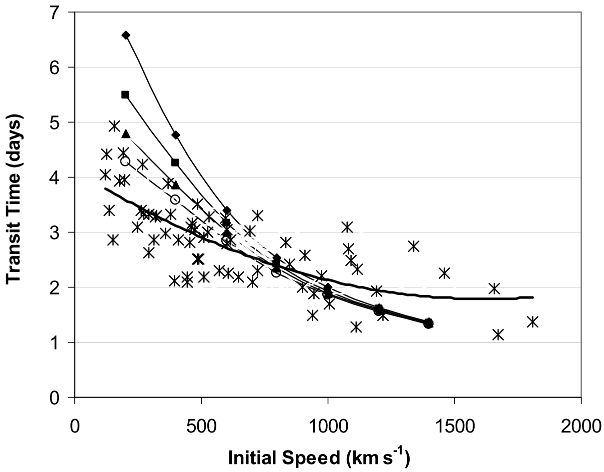

Figure 9 Comparison of the model results (Equation (7) with $\alpha_1 = 1 \times 10^{-3}\ \mathrm{s}^{-1}$, and $\beta = 1.5$) with the observed values (cross symbol) of non-interacting CMEs. A polynomial fit to the observed values is also drawn as black solid line. Thin lines joining the symbols are the same as in Figure 4 (diamond – $w_0 = 300\ \mathrm{km\,s}^{-1}$, square – $w_0 = 400\ \mathrm{km\,s}^{-1}$, triangle – $w_0 = 500\ \mathrm{km\,s}^{-1}$, circle – $w_0 = 600\ \mathrm{km\,s}^{-1}$).

the model presented herein (Figures 9 and 10). Figure 9 shows that the model values are in a quite good agreement with the observations for low-speed as well as for high-speed ICMEs ($v_0 = 300-2000\ \mathrm{km\,s}^{-1}$). There are slight deviations for the initially slow CMEs ($v_0 < 500\ \mathrm{km\,s}^{-1}$) that are traveling in the slow solar wind ($\approx 300-400\ \mathrm{km\,s}^{-1}$). If we increase the speed of the solar wind, then both results (model values and observed values) agree for both the low and the high initial speed CMEs. In the same way, as shown in Figure 10, there are no large deviations between the model and observational results in the case of interacting events. However, a large scatter of points can be seen in this case, which may be attributed to the fact that the interacting CMEs change their trend (Manoharan *et al.*, 2004), and they do not behave according to aerodynamic drag.

Similarly, we have compared the model results from the quadratic speed dependence calculations with the observed values and they are shown in Figure 11. As seen in these graphs, the model results are in better agreement with the observed values for non-interacting events of both low and high initial speed. The difference of transit-time curves for different wind speeds at the high initial-speed region (in contrast to the merging of all the transit-time curves obtained using the linear drag equation, Figures 11 and 12) covers a wide range the observed data points. Similarly, the observed values for interacting CMEs match with the model results when ($v_0 > 500\ \mathrm{km\,s}^{-1}$) and differ slightly from the model results when ($v_0 < 500\ \mathrm{km\,s}^{-1}$).

4. Conclusion

The speed of a CME as a function of the heliocentric distance [$v(R)$] is modeled using the equations of motion proposed by Vršnak and Gopalswamy (2002). A CME is accelerated or decelerated depending upon its initial speed [v_0] and the speed of the ambient solar wind. Eventually, the speed of the CME becomes constant, around $400\ \mathrm{km\,s}^{-1}$, which is the asymptotic solar-wind speed. If the initial speed of the CME is around $400\ \mathrm{km\,s}^{-1}$, it moves at nearly a constant speed. We extended the analysis of Vršnak and Gopalswamy (2002) and obtained more details on the dependence of the CME Sun–Earth transit time on the CME speed and the ambient solar-wind speed, for different combinations of α and β.

We obtained $v(R)$ dependencies for different values of α and β for particular values of v_0. By varying the values of α and β, for fast CMEs we found that when α increases, the

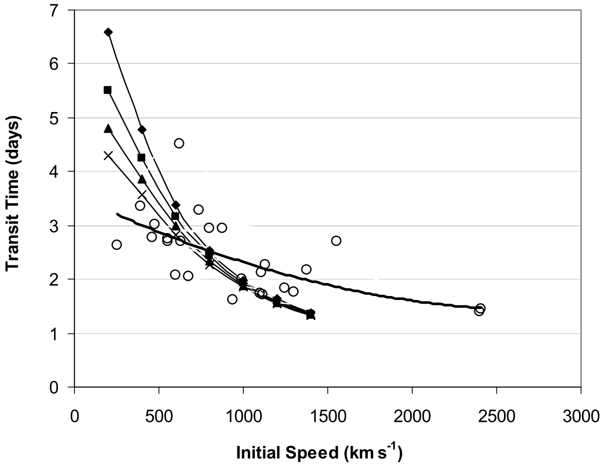

Figure 10 Comparison of the model results (Equation (7) with $\alpha_1 = 1 \times 10^{-3}\ \mathrm{s}^{-1}$, and $\beta = 1.5$) with the observed values (cross symbol) of interacting CMEs. A polynomial fit to the observed values is also drawn as black solid line. Thin lines joining the symbols are the same as in Figure 4 (diamond – $w_0 = 300\ \mathrm{km\,s^{-1}}$, square – $w_0 = 400\ \mathrm{km\,s^{-1}}$, triangle – $w_0 = 500\ \mathrm{km\,s^{-1}}$, circle – $w_0 = 600\ \mathrm{km\,s^{-1}}$).

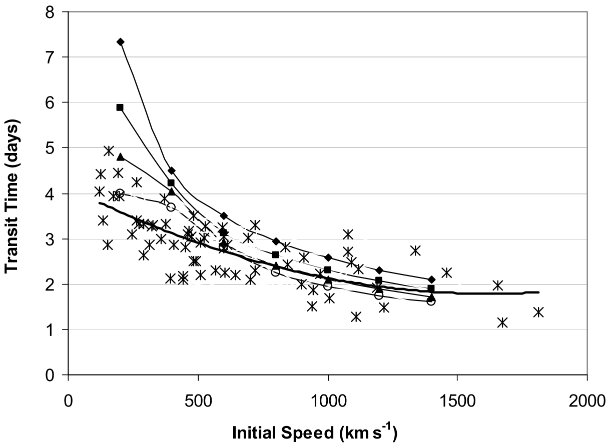

Figure 11 Comparison of the quadratic model results with the observed values (cross symbols: non-interacting CMEs). A polynomial fit to the observed values is shown as a thick line. Thin lines joining the symbols are the same as in Figure 6 (diamond – $w_0 = 300\ \mathrm{km\,s^{-1}}$, square – $w_0 = 400\ \mathrm{km\,s^{-1}}$, triangle – $w_0 = 500\ \mathrm{km\,s^{-1}}$, circle – $w_0 = 600\ \mathrm{km\,s^{-1}}$). $\alpha_2 = 5 \times 10^{-6}\ \mathrm{km}^{-1}$, and $\beta = 1.5$.

$v(R)$ curve shifts to lower speeds and when β increases, the $v(R)$ curve shifts to higher speeds. Also we have evaluated the transit time of the CMEs to reach the Earth. As a first result, we see that when the initial speed is high, the CME takes less time to reach the Earth. When α increases, the transit time increases, and when β increases, the transit time of CME decreases.

It is also found that when the wind speed is higher, the transit time of the CME is lower. When the CME initial speed is greater than $1000\ \mathrm{km\,s^{-1}}$, the effect of solar wind on the CME transit time becomes less important.

When the model results are compared with the observed values of non-interacting CMEs, we found that they are consistent from low up to high initial speeds. Especially, it is found that the quadratic model results are in better agreement with the observations. For interacting CMEs, the deviations between the model and observed values are larger than for non-interacting CMEs, which may be attributed to the momentum transfer between the two interacting CMEs. In such a case, the propagation can be modeled in two stages, *i.e.* before and after interaction.

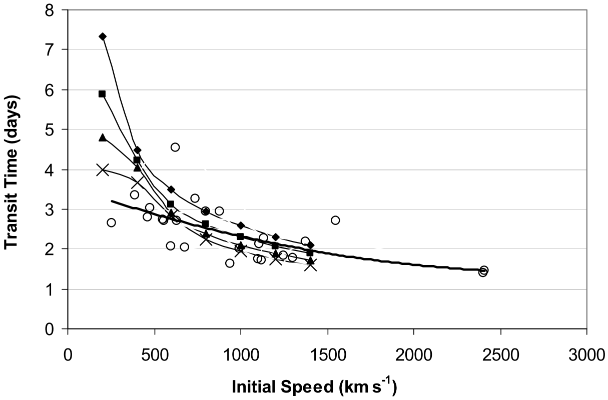

Figure 12 Comparison of the quadratic model results with the observed values (circles: interacting CMEs). A polynomial fit to the observed values is shown as a thick line. Thin lines joining the symbols are the same as in Figure 6 (diamond – $w_0 = 300\ \mathrm{km\,s^{-1}}$, square – $w_0 = 400\ \mathrm{km\,s^{-1}}$, triangle – $w_0 = 500\ \mathrm{km\,s^{-1}}$, circle – $w_0 = 600\ \mathrm{km\,s^{-1}}$). $\alpha_2 = 5 \times 10^{-6}\ \mathrm{km^{-1}}$, and $\beta = 1.5$.

Acknowledgements AS acknowledges funding from UGC, Govt. of India for minor research project (F.MRP-3330/10 (MRP/UGC-SERO)). BV acknowledges funding from the European Union Seventh Framework Programme (FP7/2007-2013) under grant agreement No. 263252 [COMESEP].

References

Borgazzi, A., Lara, A., Echer, E., Alves, M.V.: 2009, *Astron. Astrophys.* **498**, 885.
Bothmer, V., Schwenn, R.: 1995, *J. Geomagn. Geoelectr.* **47**, 1127.
Cargill, P.J.: 2004, *Solar Phys.* **221**, 135. doi:10.1023/B:SOLA-0000033366-10725-a2.
Gopalswamy, N.: 2004, In: Poletto, G., Suess, S. (eds.) *The Sun and the Heliosphere as an Integrated System*. *ASSL Series*, Kluwer, Boston, 201. Chapter 8.
Gopalswamy, N., Lara, A., Lepping, R.P., Kaiser, M.L., Berdichevsky, D., St Cyr, O.C.: 2000, *Geophys. Res. Lett.* **27**, 145.
Gopalswamy, N., Lara, A., Yashiro, S., Kaiser, M.L., Howard, R.A.: 2001, *J. Geophys. Res.* **106**, 29207.
Gopalswamy, N., Yashiro, S., Liu, Y., Michalek, G., Vourlidas, A., Kaiser, M.L., Howard, R.A.: 2005, *J. Geophys. Res.* **110**. doi:10.1029/2004JA010958.
Gosling, J.T., Bame, S.J., McComas, D.J., Phillips, J.L.: 1990, *Geophys. Res. Lett.* **17**, 901.
Koskinen, H.E.J., Huttunen, K.E.J.: 2006, *Space Sci. Rev.* **124**, 169.
Manoharan, P.K.: 2006, *Solar Phys.* **235**, 345. doi:10.1007/s11207-006-0100-y.
Manoharan, P.K., Gopalswamy, N., Yashiro, S., Lara, A., Michalek, G., Howard, R.A.: 2004, *J. Geophys. Res.* **109**.
Michalek, G., Gopalswamy, N., Lara, A., Manoharan, P.K.: 2004, *Astron. Astrophys.* **423**, 729.
Sheeley, N.R. Jr., Wang, Y.-M., Hawley, S.H., Brueckner, G.E., Dere, K.P., Howard, R.A., *et al.*: 1997, *Astrophys. J.* **484**, 472.
Temmer, M., Rollett, T., Möstl, C., Veronig, A.M., Vršnak, B., Odstrčil, D.: 2011, *Astrophys. J.* **743**, 101.
Tsurutani, B.T., Gonzalez, W.D.: 1998, In: Suess, S.T., Tsurutani, B.T. (eds.) *Magnetic Storms*, *Geophys. Monogr.* **98**, AGU, Washington, 57.
Vršnak, B.: 2001, *Solar Phys.* **202**, 173. ADS:2001SoPh..202..173V, doi:10.1023/A:1011833114104.
Vršnak, B.: 2006, *Adv. Space Res.* **38**, 431.
Vršnak, B., Gopalswamy, N.: 2002, *J. Geophys. Res.* **107**. doi:10.1029/2001/JA000120.
Vršnak, B., Magdalenic, J., Zlobec, P.: 2004, *Astron. Astrophys.* **413**, 753.
Vršnak, B., Vrbanec, D., Calogovic, J.: 2008, *Astron. Astrophys.* **490**, 811.
Vršnak, B., Zic, T.: 2007, *Astron. Astrophys.* **472**, 937.
Vršnak, B., Žic, T., Falkenberg, T.V., Möstl, C., Vennerstrom, S., Vrbanec, D.: 2010, *Astron. Astrophys.* **512**, 43.
Yashiro, S., Gopalswamy, N., Michalek, G., St Cyr, O.C., Plunkett, S.P., Rich, N.B., Howard, R.A.: 2004, *J. Geophys. Res.* **109**(A7), A07105.
Zhang, J., Dere, K.P., Howard, R.A., Bothmer, V.: 2003, *Astrophys. J.* **582**, 520.